Quasi-Two-Dimensional Calculation Of Nonequilibrium Faraday MHD Generator

Author(s): Y. Inui, T. Hara, M. Ishikawa, and J. Umoto

Session Name: Generators B

SEAM: 28 (1990)

SEAM EDX URL: https://edx.netl.doe.gov/dataset/seam-28

EDX Paper ID: 1433

QUASI-TWO-DIMENSIONAL CALCULATION OF NONEQUILIBRIUM FARADAY MHD GENERATOR

Yoshitaka Inui, Takehisa Hara, Motoo Ishikawa and Juro Umoto
Department of Electrical Engineering, Kyoto University
Yoshida-Honmachi, Sakyo-ku, Kyoto 606, Japan

ABSTRACT

To theoretically explain the experimentally obtained performance characteristics of nonequilibrium Faraday MHD generator, the authors have newly developed a quasi-two-dimensional time-dependent simulation code, in which not only the two-dimensional distributions of the electrical quantities but also the one-dimensional distributions of the gas dynamical quantities are calculated simultaneously and the interactions between electrical and gas dynamical quantities are taken into account. No model of ionization instabilities is used. The simulation results are compared with the experimental results and it is confirmed that the simulation code can predict the performance characteristics of the generator. Next, numerically obtained distributions of the electrical and gas dynamical quantities in the generator channel are described in detail. The comparison between numerical results and experiments shows that the behavior of nonequilibrium Faraday MHD generator can be well predicted when the time-dependent quasi-two-dimensional interactions between electrical and gas dynamical quantities are taken into account.

INTRODUCTION

Two-dimensional time-dependent simulations of the electrical quantities in a nonequilibrium Faraday MHD generator channel have been performed by the authors and many items about the discharge structure in the channel have been made clear[1,2]. The simulations, however, could not fully explain the experimentally obtained performance characteristics of the generator[3-6] such as the values of each electrode current and total output power, because the gas dynamical quantities were assumed to be constant in space and time and the interactions between the electrical and gas dynamical quantities were not taken into account. The authors newly develop a quasi-two-dimensional time-dependent simulation code for a nonequilibrium Faraday MHD generator channel, in which not only the two-dimensional distributions of the electrical quantities but also the one-dimensional distributions of the gas dynamical quantities are calculated simultaneously and the interactions are taken into account, to theoretically explain the experimentally obtained performance characteristics.

In this paper, at first, the numerical procedures of the newly developed quasi-two-dimensional time-dependent simulation code for a nonequilibrium Faraday MHD generator are described.

To confirm that the simulation code can predict the performance characteristics of the generator, numerical calculations are performed for the same conditions as used in the experiments performed by Harada, Shioda, et al.[5,6] (Tokyo Institute of Technology), where they used shock tube and Faraday generator driven by cesium seeded helium plasma. The numerical results are then compared with the experimental results.

Next, distributions of electrical and gas dynamical quantities in the channel are described in detail, whereas the experiments could not show the distributions because of the difficulty of their measurement. It is intended to reveal the relations between the numerically obtained distributions and the experimentally obtained performance characteristics.

BASIC EQUATIONS

Cesium seeded helium plasma is selected as the working fluid of the MHD generator in this study. Both gas dynamical and electrical properties of the plasma are calculated simultaneously to make clear the performance characteristics of the generator. The basic equations should include the equations which can determine both gas dynamical and electrical quantities.

The governing equations of gas dynamical quantities are given by the following conservation equations[7].

Mass conservation:

$$\frac{\partial \rho}{\partial t} + \nabla\cdot(\rho u) = 0 \tag{1}$$

Momentum conservation:

$$\rho\left(\frac{\partial}{\partial t} + u\cdot\nabla\right)u = -\nabla p + \nabla\cdot\tau + J\times B \tag{2}$$

Energy conservation:

$$\rho\left(\frac{\partial}{\partial t} + u\cdot\nabla\right)\left(h + \frac{u^2}{2}\right) = \frac{\partial p}{\partial t} + \nabla\cdot(\tau\cdot u - q) + J\cdot E \tag{3}$$

where

$$p = \rho RT \tag{4}$$

$$h = c_p T \tag{5}$$

The governing equations of electrical quantities are given by the following set[2,8] under the usual MHD approximations, i.e., the low magnetic Reynolds number, the charge neutrality, the single ionization and the three body recombination of helium and cesium.

Generalized Ohm's law:

$$J + \frac{\beta}{B}(J \times B) = \sigma(E^* + \frac{\nabla p_e}{e n_e}) \tag{6}$$

Maxwell's equations:

$$\nabla \cdot J = 0 \tag{7}$$

$$\nabla \times E = 0 \tag{8}$$

Continuity of ions:

$$\frac{\partial n_{ih}}{\partial t} + \nabla \cdot (n_{ih} u) = k_{fh} n_e n_h - k_{rh} n_e^2 n_{ih} \tag{9}$$

$$\frac{\partial n_{ic}}{\partial t} + \nabla \cdot (n_{ic} u) = k_{fc} n_e n_c - k_{rc} n_e^2 n_{ic} \tag{10}$$

Charge neutrality:

$$n_e = n_{ih} + n_{ic} \tag{11}$$

Electron energy conservation:

$$\begin{aligned} &\frac{\partial}{\partial t}\{n_{ih}(\tfrac{3}{2}kT_e + \varepsilon_{ih}) + n_{ic}(\tfrac{3}{2}kT_e + \varepsilon_{ic})\} \\ &+ \nabla \cdot [\{n_{ih}(\tfrac{3}{2}kT_e + \varepsilon_{ih}) \\ &+ n_{ic}(\tfrac{3}{2}kT_e + \varepsilon_{ic})\} u_e] \\ &= J \cdot E^* - \nabla \cdot (p_e u_e) - Q_R \\ &- \tfrac{3}{2}\delta n_e m_e k (T_e - T)(\frac{\nu_h}{m_h} + \frac{\nu_c}{m_c} + \frac{\nu_{ih}}{m_h} + \frac{\nu_{ic}}{m_c}) \end{aligned} \tag{12}$$

where

$$\left.\begin{aligned} &\sigma = \frac{e^2 n_e}{m_e \nu_e}, \qquad && \beta = \frac{eB}{m_e \nu_e} \\ &E^* = E + u \times B, && J = e n_e (u - u_e) \\ &p_e = n_e k T_e, && \nu_e = \nu_h + \nu_c + \nu_{ih} + \nu_{ic} \end{aligned}\right\} \tag{13}$$

QUASI-TWO-DIMENSIONAL TIME-DEPENDENT SIMULATION CODE FOR FARADAY GENERATOR

The schematic diagram of Faraday MHD generator and the coordinate system used in the analysis are shown in Fig. 1. In the code, not only the two-dimensional distributions of the electrical quantities in x-y plane but also the one-dimensional distributions of the gas dynamical quantities along x-direction are calculated and the interactions between the electrical and gas dynamical quantities are taken into account.

At first, the following assumptions are introduced[8,9].

(1) All quantities are constant in z-direction.

$$\frac{\partial}{\partial z} = 0 \tag{14}$$

(2) The gas velocity has only the x-component and is represented as the following form:

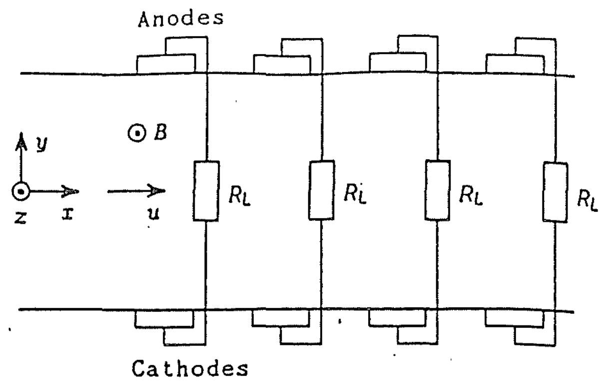

Fig. 1 Schematic diagram of Faraday MHD generator.

$$u = (u_x, 0, 0) \tag{15}$$

(3) The magnetic field is constant in time and has the form:

$$B = (0, 0, B_z) \tag{16}$$

(4) The term $\nabla p_e / e n_e$ in Ohm's law is negligible.

(5) All terms including space derivatives in the electron energy conservation equation are negligible compared to the term of Joule heating.

(6) The relaxation of electron temperature is instantaneous compared to the relaxation of electron density.

The gas flow is assumed to consist of the core flow and the boundary layer. In the core flow, the gas dynamical quantities (ρ, u, p, T, h) are assumed to be constant in not only z-direction but also in y-direction and vary only in x-direction.

$$\frac{\partial}{\partial y} = \frac{\partial}{\partial z} = 0 \tag{17}$$

Considering this assumption together with the above assumptions (1)-(3), the governing equations of gas dynamical quantities (1)-(3) are transformed into the following one-dimensional equations[10] in the core flow:

$$\frac{\partial U}{\partial t} + \frac{\partial F}{\partial x} - C = 0 \tag{18}$$

$$\left.\begin{aligned} &U = \begin{bmatrix} \rho \\ m_x \\ \varepsilon_s \end{bmatrix}, \quad F = \begin{bmatrix} m_x \\ m_x^2/\rho + p \\ m_x(\varepsilon_s + p)/\rho \end{bmatrix} \\ &C = -\frac{1}{A}\frac{\partial A}{\partial x}\begin{bmatrix} m_x \\ m_x^2/\rho \\ m_x(\varepsilon_s + p)/\rho \end{bmatrix} - \begin{bmatrix} 0 \\ f \\ q \end{bmatrix} \\ &\qquad + \begin{bmatrix} 0 \\ \overline{J_y B_z} \\ \overline{J_x E_x + J_y E_y} \end{bmatrix} \\ &m_x = \rho u_x, \quad \varepsilon_s = \rho(h + u_x^2/2 - p/\rho) \\ &\overline{J_y} = \frac{1}{h_y}\int_0^{h_y} J_y dy \\ &\overline{J_x E_x + J_y E_y} = \frac{1}{h_y}\int_0^{h_y}(J_x E_x + J_y E_y) dy \end{aligned}\right\} \tag{19}$$

The following MacCormack's predictor-corrector method[11] is adopted to solve Eq. (18).

$$\left.\begin{aligned} U_i^{\overline{n}} &= U_i^n - \Delta t\left(\frac{F_{i+1}^n - F_i^n}{\Delta x} - C_i^n\right) \\ U_i^{n+1} &= \frac{1}{2}\left\{U_i^n + U_i^{\overline{n}} - \Delta t\left(\frac{F_i^{\overline{n}} - F_{i-1}^{\overline{n}}}{\Delta x} - C_i^{\overline{n}}\right)\right\} \end{aligned}\right\} \quad (20)$$

where subscript i and superscript n designate the x coordinate point and time mark, respectively. Symbols F_i^n and C_i^n designate F and C when the various gas dynamical quantities are given by U_i^n.

The gas dynamical quantities in the boundary layer are estimated by using a constant boundary layer thickness and the (1/n)-th power law, whereas those in the core flow are calculated by Eq. (18).

Considering the assumptions (1)-(6) and introducing the electrical potential φ defined as

$$E_x = -\frac{\partial \varphi}{\partial x}, \qquad E_y = -\frac{\partial \varphi}{\partial y} \quad (21)$$

the governing equations of electrical quantities (6)-(12) are transformed into the following two-dimensional equations[8,9].

$$J_x = \frac{\sigma}{1+\beta^2}\{E_x - \beta(E_y - u_x B_z)\} \quad (22)$$

$$J_y = \frac{\sigma}{1+\beta^2}\{\beta E_x + (E_y - u_x B_z)\} \quad (23)$$

$$\frac{\partial}{\partial x}\left\{w_z \frac{\sigma}{1+\beta^2}\left(-\frac{\partial \varphi}{\partial x} + \beta\frac{\partial \varphi}{\partial y} + \beta u_x B_z\right)\right\} + \frac{\partial}{\partial y}\left\{w_z \frac{\sigma}{1+\beta^2}\left(-\beta\frac{\partial \varphi}{\partial x} - \frac{\partial \varphi}{\partial y} - u_x B_z\right)\right\} = 0 \quad (24)$$

$$\frac{\partial n_{ih}}{\partial t} + u_x\frac{\partial n_{ih}}{\partial x} = \dot{n}_{ih} + \frac{n_{ih}}{\rho}\left(\frac{\partial \rho}{\partial t} + u_x\frac{\partial \rho}{\partial x}\right) \quad (25)$$

$$\frac{\partial n_{ic}}{\partial t} + u_x\frac{\partial n_{ic}}{\partial x} = \dot{n}_{ic} + \frac{n_{ic}}{\rho}\left(\frac{\partial \rho}{\partial t} + u_x\frac{\partial \rho}{\partial x}\right) \quad (26)$$

$$n_e = n_{ih} + n_{ic} \quad (27)$$

$$\frac{2}{3kn_e}\frac{J_x^2 + J_y^2}{\sigma} - \delta m_e(T_e - T) \times \left(\frac{\nu_h}{m_h} + \frac{\nu_c}{m_c} + \frac{\nu_{ih}}{m_h} + \frac{\nu_{ic}}{m_c}\right) - \left(T_e + \frac{2\varepsilon_{ih}}{3k}\right)\frac{\dot{n}_{ih}}{n_e} - \left(T_e + \frac{2\varepsilon_{ic}}{3k}\right)\frac{\dot{n}_{ic}}{n_e} - Q_R = 0 \quad (28)$$

where

$$\dot{n}_{ih} = k_{fh} n_e n_h - k_{rh} n_e^2 n_{ih} \quad (29)$$

$$\dot{n}_{ic} = k_{fc} n_e n_c - k_{rc} n_e^2 n_{ic} \quad (30)$$

In the code, Galerkin finite element method[8] with the rectangular bilinear element is used to calculate the electrical potential φ with Eq. (24). On the characteristic curves given by

$$\frac{dx}{dt} = u_x, \qquad \frac{du}{dt} = 0 \quad (31)$$

Eqs. (25) and (26) result in the following forms.

$$\frac{dn_{ih}}{dt} = \dot{n}_{ih} + \frac{n_{ih}}{\rho}\frac{d\rho}{dt} \quad (32)$$

$$\frac{dn_{ic}}{dt} = \dot{n}_{ic} + \frac{n_{ic}}{\rho}\frac{d\rho}{dt} \quad (33)$$

The ion densities n_{ih} and n_{ic} are calculated with these equations. The electron temperature T_e is calculated with Eq. (28) by Newton-Raphson method.

COMPARISON WITH EXPERIMENTAL RESULTS

In this chapter, the calculation results obtained by the newly developed quasi-two-dimensional time-dependent simulation code explained in the preceding chapter are compared with the experimental results to confirm that the code can predict the performance characteristics of nonequilibrium Faraday MHD generator. The results obtained by a series of experiments performed by Harada, Shioda, et al.[5,6] (Tokyo Institute of Technology) using shock tube and Faraday generator driven by cesium seeded helium plasma are selected as the experimental data to be compared. The calculations are performed for the región between the channel throat and the last electrodes pair of the experimentally used generator channel. The dimensions and the cross sectional view of the calculated channel are shown in Table 1 and Fig. 2, respectively. Simulations are performed in 8

Table 1 Dimensions of calculated generator.

Channel length	41 cm	
Channel height	7 cm	
Channel width	2 + 0.1x cm	
Nozzle length	6 cm	
Electrode pitch	1 cm	
Electrode width	0.4 cm	
Number of electrodes	35	
Magnetic flux density	1.1 + x/6 T	(x < 6 cm)
	2.1 T	(x ≥ 6 cm)

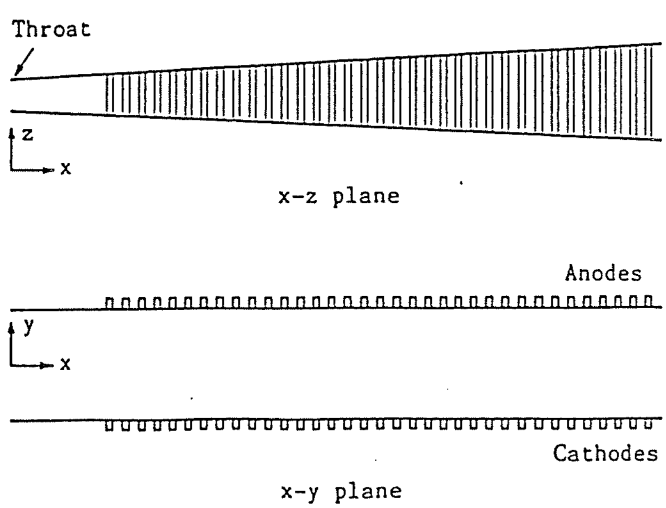

Fig. 2 Cross sectional view of calculated generator.

Table 2 Numerical conditions.

Case No.	Inlet stagnation temperature	Inlet stagnation pressure	Load resistance
1	1950 K	1.7 atm	5 Ω
2	1950 K	1.7 atm	7 Ω
3	1950 K	1.7 atm	10 Ω
4	1950 K	1.7 atm	15 Ω
5	1950 K	1.7 atm	30 Ω
6	1950 K	1.7 atm	50 Ω
7	2000 K	1.5 atm	7 Ω
8	2200 K	1.3 atm	7 Ω

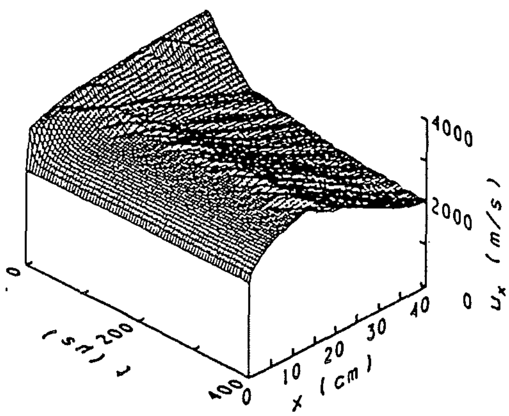

Gas velocity u_x.

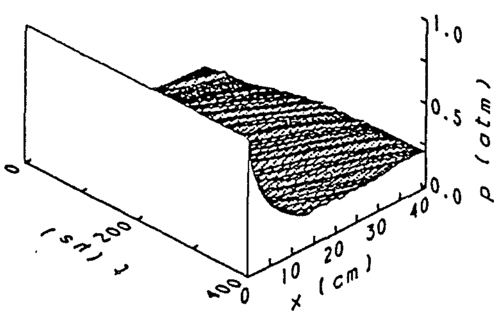

Gas pressure p.

Fig. 3 Transient distributions of gas dynamical quantities along x-direction.

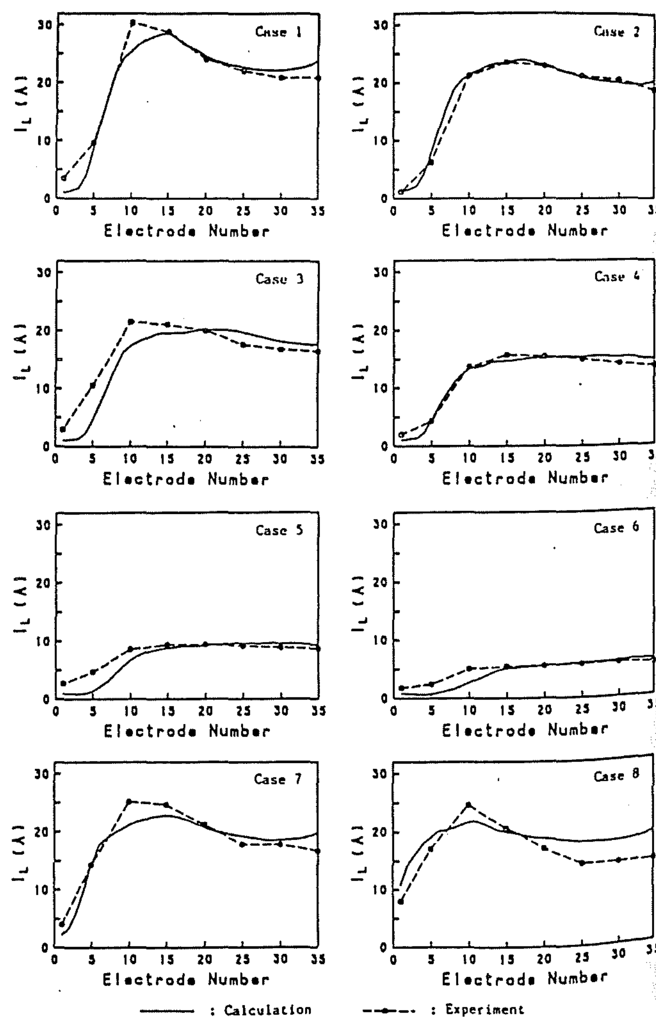

Fig. 4 Load current distributions obtained by calculations and experiments.

cases of conditions shown in Table 2, all of which are the same as used in the experiments. The seed fraction is selected as $\varepsilon = 8\times10^{-5}$ in all cases. Since the channel throat is selected as the inlet of the calculated region, the inlet Mach number is fixed as

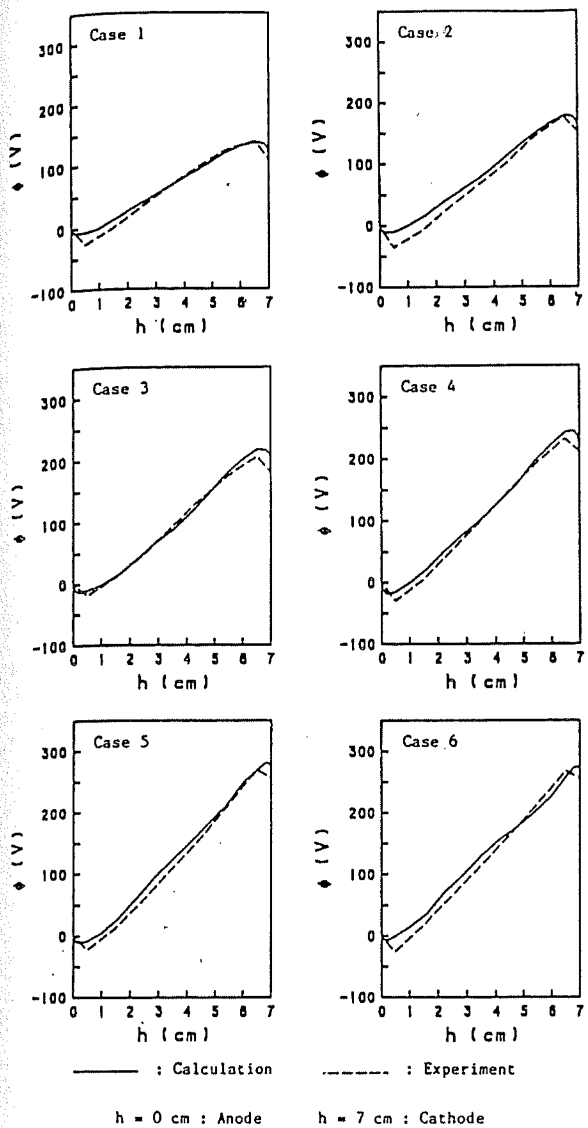

Fig. 5 Potential distributions obtained by calculations and experiments.

Table 3 Total output powers obtained by calculations and experiments.

Case No.	Total output power	
	Calculation	Experiment
1	87.0 kW	89.4 kW
2	94.6 kW	92.0 kW
3	100.4 kW	106.8 kW
4	93.5 kW	91.5 kW
5	66.1 kW	70.1 kW
6	40.3 kW	44.4 kW
7	88.2 kW	91.8 kW
8	87.5 kW	72.7 kW

N = 1. In the calculations, steady state distributions of the gas dynamical quantities in the case of no magnetic flux density are used as initial conditions of them. It is also assumed that there exist boundary layers of 10 mm near the anode and cathode walls in which the profiles of gas velocity and gas temperature are given by the (1/7)-th power law.

As examples of time-dependent distributions of the quantities in the generator, Fig. 3 shows the distributions of gas velocity u_r and gas pressure p in Case 3. This figure tells that the distributions attain to the steady state by t = 300 μs. Considering this result and the fact that the experimental data are the time averaged values at the steady state, the calculation is performed until t = 400 μs and the time averaged values from t = 300 μs to t = 400 μs are adopted as the calculated data to be compared with the experimental data. The distributions of load current of each electrodes pair, the potential distributions at 20th electrodes pair and the total output powers obtained by both the calculations and the experiments in the above 8 cases are shown in Figs. 4, 5 and Table 3, respectively. Since the potential distributions in Case 7 and Case 8 are not measured in the experiments, no graphs are shown in the cases in Fig. 5. These figures and table reveal that the numerically obtained results agree well with the experimental results, showing that the newly developed quasi-two-dimensional time-dependent simulation code can predict the performance characteristics of linear generator.

DISTRIBUTIONS OF ELECTRICAL AND GAS DYNAMICAL QUANTITIES

Details of electrical and gas dynamical quantities in nonequilibrium Faraday MHD generator were not sufficiently made clear by the experiments because of the difficulty of their measurement. It is, however, indispensable to grasp these distributions in detail for further researches such as the design of large scale generator channel. On the other hand, it was made clear in the preceding chapter that the calculation results of the performance characteristics obtained by the newly developed quasi-two-dimensional time-dependent simulation code agree well with the experimental results, indicating that the code can also simulate the distributions of the electrical and gas dynamical quantities in the generator fairly well because the distributions determine the performance characteristics. The distributions of electrical and gas dynamical quantities in the generator obtained by the calculations are thus described in this chapter and it is also intended to reveal the relations between the numerically obtained distributions and the experimentally obtained performance characteristics.

Figures 6-8 show the distributions of current, electron temperature and electron density, respectively, at the steady state (t = 400 μs) in Case 1 (R_L = 5 Ω), Case 3 (R_L = 10 Ω), Case 4 (R_L = 15 Ω) and Case 6 (R_L = 50 Ω). Effects of load change can be also studied because all conditions except the load resistance are kept the same in these 4 cases. Figures 7 and 8 depict the distributions only in the half region of the channel between the channel center line and the anode wall to clearly show the distributions along the center line of the channel. These figures show that the current distribution in the channel is inhomogeneous by the ionization instability of the plasma[12,13] and there exist high

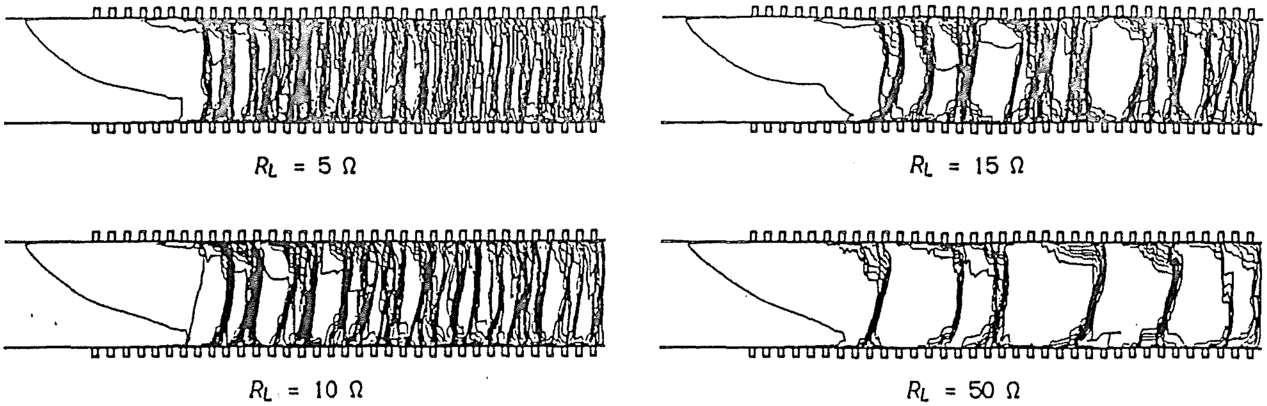

(ΔΨ = 3 A)

Fig. 6 Current distributions in the generator.

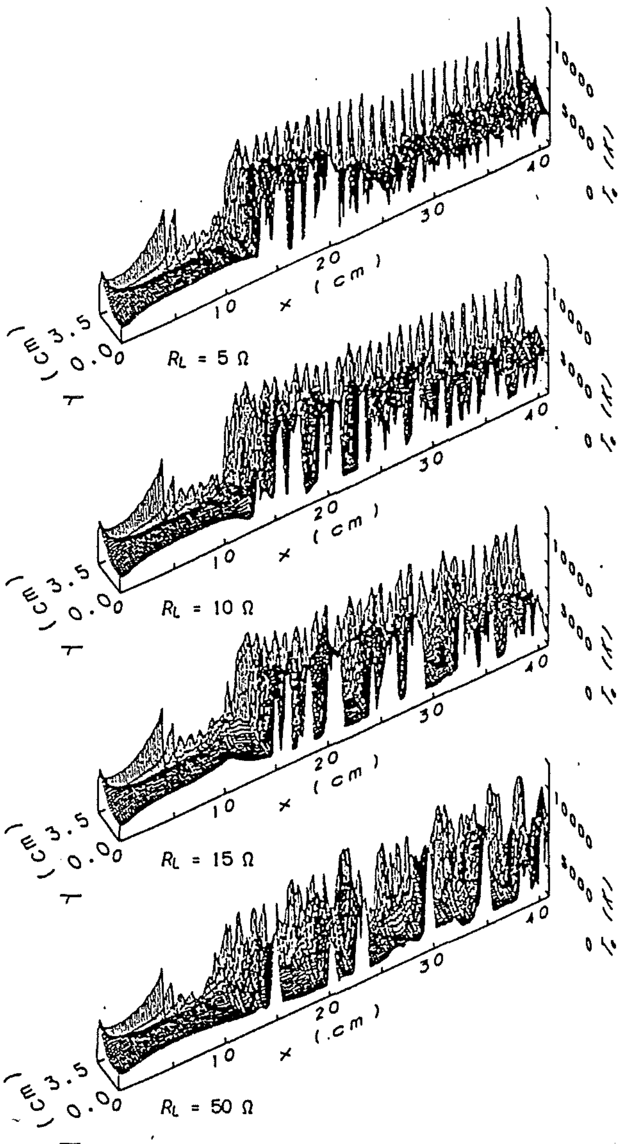

Fig. 7 Electron temperature distributions in the generator.

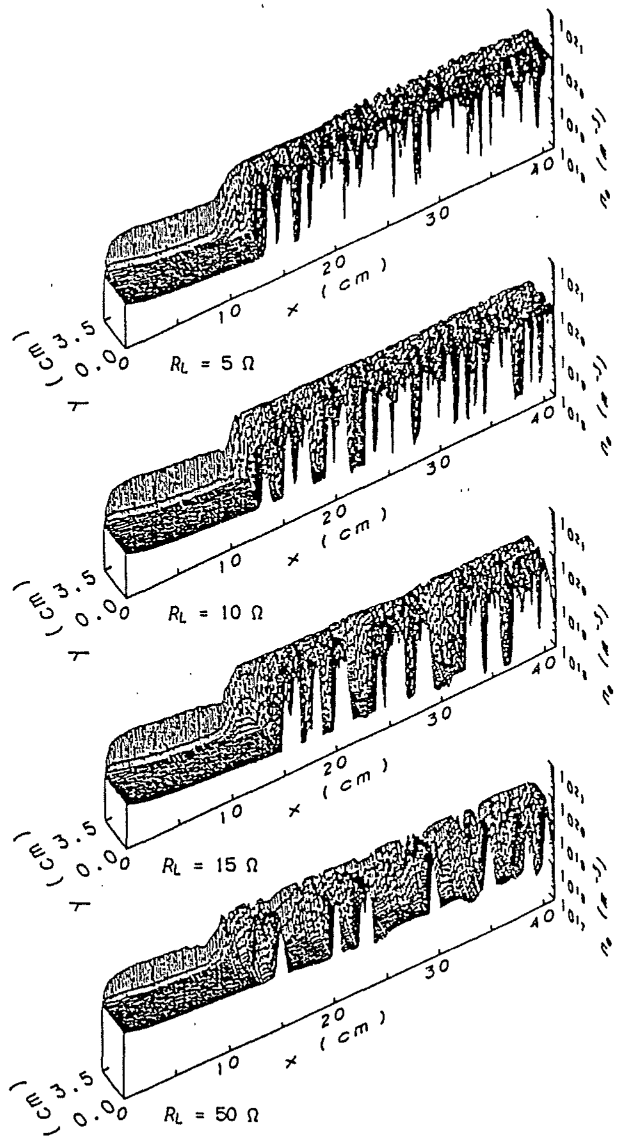

Fig. 8 Electron density distributions in the generator.

current density regions called streamer regions and low current density regions in the channel. The width of the streamers becomes narrow and their pitch becomes wide as the load resistance becomes high. Both the electron temperature and the electron density are high in the streamer regions. There exist layers of high electron density near the electrode walls. These layers are formed because the current flowing into or out of the fixed electrodes heats the flowing plasma and the nonequilibrium ionization occurs there. The high electron density indicates high conductivity in the boundary layer, leading to small electrode voltage drop in nonequilibrium MHD generator as shown in Fig. 5. Since the voltage drop is usually much larger in such a small scale open cycle MHD generator[4], there exists an advantage in nonequilibrium MHD generator compared to the open cycle MHD generator that higher performance characteristics can be obtained from smaller scale generator channel.

Figure 9 shows the distributions of gas dynamical quantities in the same 4 cases (R_L = 5, 10, 15 and 50 Ω) at the steady state (t = 400 μs). It is made clear that the inhomogeneity of distributions of the electrical quantities has effects upon the gas dynamical quantities, resulting in the fluctuation in the channel. The gas temperature distribution significantly fluctuates, whereas the gas velocity distribution is relatively smooth. This means that the energy interaction between the electrical and gas dynamical quantities is much larger than the momentum interaction. The interactions become high as the load resistance becomes small. Shock wave, therefore occurs in the channel and the gas flow becomes subsonic after the shock when R_L = 5 Ω, whereas the gas velocity does not decrease even at the latter half of the channel when R_L = 50 Ω. The occurrence of shock wave is the reason the load current decreases at the latter half of the channel in the case R_L = 5 Ω (Case 1) as seen in Fig. 4. The outlet Mach number is about 1 when R_L = 10 Ω. This is the reason the largest output power is obtained in this case (Case 3) as seen in Table 3, because the outlet Mach number of about 1 means that the interaction is the optimum and the most effective generation is realized in the given generator configuration.

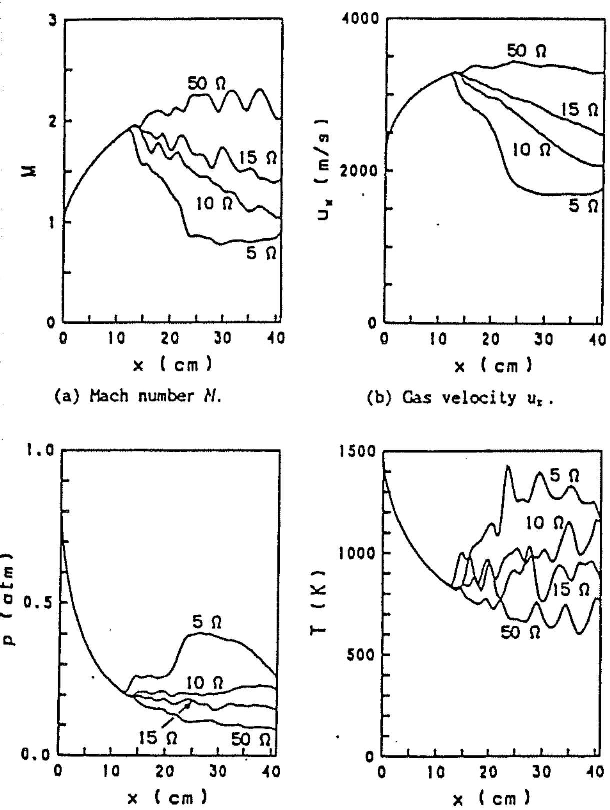

(a) Mach number M.

(b) Gas velocity u_x.

(c) Gas pressure p.

(d) Gas temperature T.

Fig. 9 Distributions of gas dynamical quantities in the generator.

CONCLUSIONS

The numerical procedures of the quasi-two-dimensional time-dependent simulation code for a nonequilibrium Faraday MHD generator are described at first. The code is newly developed by the authors to intend to theoretically explain the experimentally obtained performance characteristics of the generator.

The numerical simulations are performed for the same conditions as used in the experiments performed by Harada, Shioda, et al. (Tokyo Institute of Technology) using shock tube and Faraday generator driven by cesium seeded helium plasma. The numerically obtained distributions of load current of each electrodes pair, potential distributions at 20th electrodes pair and total output powers are compared with the experimental results and it is confirmed that the code can predict the performance characteristics of the generator.

Numerically obtained distributions of current, electron temperature, electron density and gas dynamical quantities in the generator at the steady state are described and the relations are also made clear between the numerically obtained distributions and the experimentally obtained performance characteristics, which are required for further research.

ACKNOWLEDGMENTS

The authors would like to express their grateful thanks to Professor S. Shioda and Dr. N. Harada of Tokyo Institute of Technology for the offer of their experimental data on nonequilibrium Faraday MHD generator. The computations were done on the FACOM M782/VP400 at the Data Processing Center, Kyoto University.

REFERENCES

1. T. Hara, J. Umoto and Y. Inui: "Streamer Structure in Noble Gas MHD Channels", Proceedings of 5th Symposium on Efficient Use of Energy and Direct Electrical Power Generation, pp. S2.2.1-S2.2.15 (1983).
2. T. Hara, J. Umoto and Y. Inui: "Numerical Analysis of the Nature of the Streamers in Noble Gas MHD Generator", Proceedings of 8th International Conference on MHD Electrical Power Generation, Vol. 4, pp. 136-139 (1983).
3. W. J. M. Balemans and L. H. Th. Rietjens: "High Enthalpy Extraction Experiments with the Eindhoven Blow-Down Facility", Proceedings of 9th Inter-

national Conference on MHD Electrical Power Generation, Vol. 2, pp. 330-340 (1986).

4. N. Harada, et al.: "Experimental Investigation on Faraday Generator Performance with Seeded Helium", Proceedings of 9th International Conference on MHD Electrical Power Generation, Vol. 2, pp. 384-393 (1986).
5. N. Harada, et al.: "Experiments with Closed Cycle MHD Generators Driven by Cesium Seeded Helium", Proceedings of 26th Symposium on Engineering Aspects of MHD, pp. 9.1.1-9.1.12 (1988).
6. N. Harada, S. Tada, H. Yamasaki and S. Shioda: "Performance and Inlet Relaxation of a Closed Cycle Faraday MHD Generator Driven by Helium", Journal of Propulsion and Power, submitted.
7. R. J. Rosa: "Magnetohydrodynamic Energy Conversion", McGraw-Hill (1968).
8. T. Hara, A. Veefkind and L. H. Th. Rietjens: "Numerical Simulation of the Inhomogeneous Discharge Structure in Noble Gas MHD Generators", AIAA Journal, Vol. 20, No. 11, pp. 1473-1480 (1982).
9. Y. Inui, et al.: "Quasi-Two-Dimensional Calculations of the Nonequilibrium Disk Type MHD Generator", Proceedings of 9th International Conference on MHD Electrical Power Generation, Vol. 4, pp. 1598-1607 (1986).
10. D. A. Oliver: "The Time Dependent Magnetohydrodynamic Generator", Proceedings of 14th Symposium on Engineering Aspects of MHD, pp. V.5.1-V.5.9 (1974).
11. R. W. MacCormack: "The Effect of Viscosity in Hypervelocity Impact Cratering", AIAA Hypervelocity Impact Conference, AIAA Paper 69-354 (1969).
12. J. L. Kerrebrock: "Nonequilibrium Ionization Due to Electron Heating: I. Theory", AIAA Journal, Vol. 2, No. 6, pp. 1072-1080 (1964).
13. A. H. Nelson and M. G. Haines: "Analysis of the Nature and Growth of Electrothermal Waves", Plasma Physics, Vol. 11, pp. 811-837 (1969).
14. M. Ishikawa and J. Umoto: "Three-Dimensional Analysis of Faraday Type MHD Generator for Presumed Next Pilot Plant", Proceedings of 25th Symposium on Engineering Aspects of MHD, pp. 7.3.1-7.3.10 (1987).